A 2x2 MIMO Spatial Multiplexing 5G Signal Reception in a 500 km/h High-Speed Vehicle using an Augmented Channel Matrix Generated by a Delay and Doppler Profiler

Suguru Kuniyoshi[1)], Rie Saotome[1)], Shiho Oshiro[2)] and Tomohisa Wada[3)]
kuniyoshi@magnadesignnet.com
1) Magna Design Net Inc., 3-1-15 Maejima, Naha-shi, Okinawa, Japan
2) Information Technology Center, University of the Ryukyus, Okinawa, Japan
3) Dept. of Engineering, University of the Ryukyus, Senbaru 1, Nishihara, Okinawa, Japan

Summary

This paper proposes a method to extend Inter-Carrier Interference (ICI) canceling Orthogonal Frequency Division Multiplexing (OFDM) receivers for 5G mobile systems to spatial multiplexing 2x2 MIMO (Multiple Input Multiple Output) systems to support high-speed ground transportation services by linear motor cars traveling at 500 km/h. In Japan, linear-motor high-speed ground transportation service is scheduled to begin in 2027. To expand the coverage area of base stations, 5G mobile systems in high-speed moving trains will have multiple base station antennas transmitting the same downlink (DL) signal, forming an expanded cell size along the train rails. 5G terminals in a fast-moving train can cause the forward and backward antenna signals to be Doppler-shifted in opposite directions, so the receiver in the train may have trouble estimating the exact channel transfer function (CTF) for demodulation.

A receiver in such high-speed train sees the transmission channel which is composed of multiple Doppler-shifted propagation paths. Then, a loss of sub-carrier orthogonality due to Doppler-spread channels causes ICI. The ICI Canceller is realized by the following three steps. First, using the Demodulation Reference Symbol (DMRS) pilot signals, it analyzes three parameters such as attenuation, relative delay, and Doppler-shift of each multi-path component. Secondly, based on the sets of three parameters, Channel Transfer Function (CTF) of sender sub-carrier number $\boldsymbol{n}$ to receiver sub-carrier number $\boldsymbol{l}$ is generated. In case of $\boldsymbol{n} \neq \boldsymbol{l}$, the CTF corresponds to ICI factor. Thirdly, since ICI factor is obtained, by applying ICI reverse operation by Multi-Tap Equalizer, ICI canceling can be realized.

ICI canceling performance has been simulated assuming severe channel condition such as 500 km/h, 8 path reverse Doppler Shift for QPSK, 16QAM, 64QAM and 256QAM modulations. In particular, 2x2MIMO QPSK and 16QAM modulation schemes, BER (Bit Error Rate) improvement was observed when the number of taps in the multi-tap equalizer was set to 31 or more taps, at a moving speed of 500 km/h and in an 8-pass reverse doppler shift environment.

Key words:
5G, 5th Generation Mobile Communication System, MIMO, Multiple Input Multiple Output, Channel estimation, Delay and Doppler profiler, Inter-Carrier-Interference Canceller

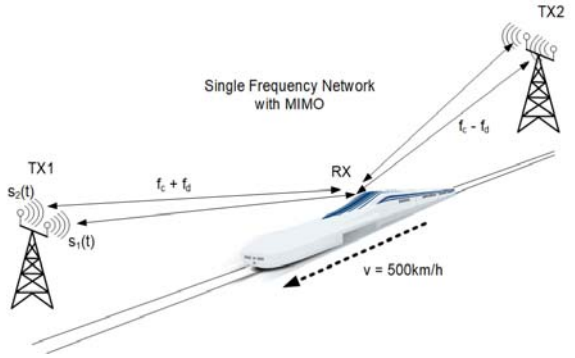

Fig. 1: Reception environment of revised Doppler shifted signals by combining signals originating from two base stations in a single frequency network with MIMO channels in the high-speed train

I. Introduction

A high-speed ground transportation service using linear motors with a speed of 500 km/h is scheduled to begin between Tokyo and Nagoya in 2027. The current top speed of the Shinkansen is 300 km/h. The maximum speed of linear motor cars, which will use magnetic levitation, will be 500 km/h. Even in trains traveling at such high speeds, there is high demand for access to rich contents, such as Internet access and watching the movie using mobile communication systems. High-speed communications are essential for accessing rich content, and demand for high-speed and stable wireless communications is constantly increasing regardless of time and location. 5G wireless communication systems can be expected to provide higher-speed, higher-capacity communications than ever before. However, wireless communications in high-speed moving trains are subject to a very severe Doppler shift environment.

To support 5G services in trains, 5G will use several different configurations compared to 4G-LTE (4th Generation Long term evolution). First, to mitigate the Doppler frequency shift, the subcarrier spacing will be increased from 15 kHz to 30 kHz. This change

Manuscript received October 5, 2023
Manuscript revised October 20, 2023
https://doi.org/10.22937/IJCSNS.2023.23.10.1

automatically shortens the OFDM symbol length by half. As a result, the performance of tracking changes in channel conditions is improved. Second, to expand the base station coverage area for mobile services, the same downlink (DL) signal is transmitted from multiple base station antennas to form an expanded cell size along the train tracks. In such a situation, the forward and backward antenna signals are Doppler shifted in opposite directions, respectively, and the receiver in the train may suffer from estimating the exact channel transfer function (CTF) for demodulation. Fig. 1 shows a situation where two DL signals are received in a vehicle. Here, f_c represents the carrier frequency. Approaching TX1 antenna signal is $(f_c + f_d)$ shifted and backward TX2 signal is $(f_c - f_d)$ shifted. In a MIMO system, spatial multiplexing is performed using two or more transmit antennas at the base station. In order to separate the spatially multiplexed signals, two or more antennas of the receiving equipment are also required. In the reference paper [1], the effectiveness of the channel estimation scheme using the Delay and Doppler Profiler (DDP) algorithm was demonstrated by computer simulations in an environment limited to the SISO (Single Input Single Output) propagation path. In this paper, we applied the channel estimation using the DDP algorithm to 2x2 MIMO with spatial multiplexing in order to achieve higher transmission data rate, and build a simulation model. In Section II, we first briefly indicate that we are targeting 5G mobile communication systems. Next, we describe the algorithm of the DDP-based ICI canceller in the proposed 2x2 MIMO signal reception environment. In Section III, we present computer simulation results. Finally, Section IV presents conclusions.

II. DDP-based ICI Canceller for 2x2 MIMO in 5G Mobile Communication Systems

The 5th generation mobile communication system [2] is an OFDM communication system standard developed as a successor to the 4G-LTE system, with various enhancements. For example, in 4G-LTE, the subcarrier spacing used in the data channel was fixed at 15 kHz, while 5G supports variable subcarrier spacing of 15/30/60/120. In the linear motor car application, a subcarrier frequency of 30 kHz is used for the 3.9 GHz RF carrier. Table I summarizes the 5G system parameters for this application, assuming 100 MHz bandwidth and 3276 subcarriers to support eMBB (enhanced mobile broadband). Since the subcarrier spacing f0 is 30 kHz, an OFDM symbol length T of 33.33 us (4096 sampling points) is used. Fig. 2 shows the 5G frame structure when f_0 is 30 kHz. This structure is a Frequency Range 1 frame structure, commonly referred to as Sub6, which is used when the center frequency is below 6 GHz. 1 frame length is 10 ms and divided into 20 Slots. In one Slot, 14 OFDM symbols are embedded. Cyclic prefix (CP) length is 288 sampling points for each 4096 points

Table 1: 5th Generation Mobile Communication System Parameters

Parameters	Value
System Band Width	100 MHz
Sub-carrier Spacing (f_0)	30 kHz
Pass Band Frequency	3.9 GHz
OFDM symbol length (T)	33.33 us (4096 points)
Number of Common Resource Blok (CRB)	273
Number of Sub-carriers	3276
Sampling Frequency (Fs)	122.88 Msps
FFT size	4096
CP length	352 or 288 points

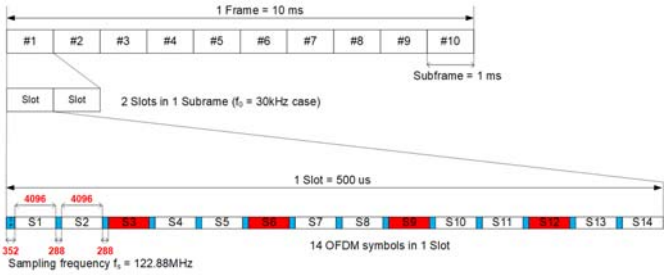

Fig. 2: 5G Frame and Slot structure

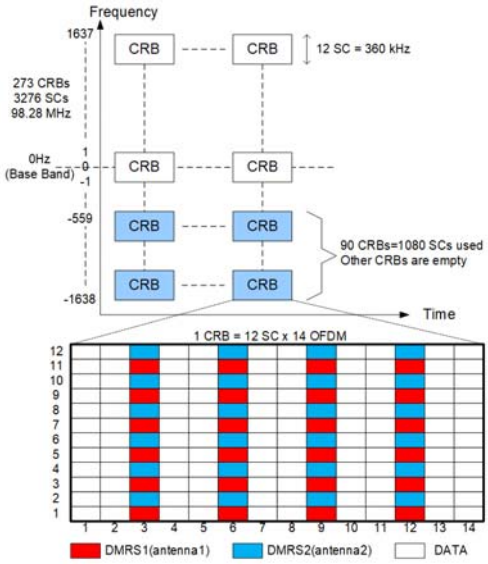

Fig. 3: Time and Frequency structure of 5G System for 2x2 MIMO

OFDM symbols except the 1st CP. The length of the 1st CP is a little expanded such as 352 points. In 5G system, Demodulation Reference Signals (DMRS) are inserted to some Sub-carriers to measure CTF and the DMRS can be placed with a high degree of freedom according to the system configuration. This time, DMRS is asserted in S3, S6, S9, S12 OFDM symbols to detect rapidly time-domain changing CTF [3].

Time-Frequency structure of this 5G system is shown in Fig. 3. Since 12 sub-carriers and 14 OFDM symbols constitute one Common Resource Block (CRB), the total 3276 sub-carriers correspond to 273 CRBs. The detail of sub-carrier arrangement in a CRB is also shown in the figure. For frequency direction (vertically), DMRS for Tx Antenna 1 are placed every 2 sub-carriers as shown in the odd number places. Similarly, DMRS for Tx Antenna 2 are placed every 2 sub-carriers as shown in the even number places.

A) Physical layer of 5G communication MIMO system

Fig. 4 shows the block diagram of the Physical Layer (PHY) of 5G 2x2 MIMO (Multiple Input Multiple Output) system. The upper side is the transmitter and the lower side is the receiver. The Bit data supplied by the upper MAC (Media Access Control), protocol and application layers are digitally modulated into QPSK / 16QAM / 64QAM / 256QAM at the Antenna mapper, and the modulated symbols are then split as different streams at each of the two transmit antennas as shown in Fig. 4. Then the modulated symbols and DMRS pilot signals for each Tx antennas configured Slots as shown in Fig. 3. Then Inverse 4096 points Fourier Transform (IFFT) is performed as OFDM modulation and CP is appended for each Tx antenna. This signal is Baseband (BB) signals. Up-conversion is applied to the BB signal to generate passband signals, which are radiated through a power amplifiers and antennas for each stream. In this paper, 2x2 MIMO refers to spatial multiplexing MIMO unless otherwise specified. Thus, 2x2 MIMO has twice the transmission capacity compared to SISO.

The receiver side is basically the reverse process of the transmitter side. However, since the receiving signal is distorted through the propagation channel, CTF, which is a Frequency domain representation of Channel Impulse Response in Time domain, has to be estimated and the distortion has to be compensated at Equalizer using the estimated CTF. In addition, signals transmitted separately at the transmitter end arrive at the receiver end after being mixed together on the propagation channel. Therefore, the CTF must be calculated for four paths in 2x2 MIMO environment, compared to the amount of CTF calculations required in SISO environment, which quadruples the amount of calculations required to find the CTF.

Conventional 5G receivers interpolate CTF values measured at DMRS locations in the frequency and time domains to obtain CTFs for all subcarrier locations; in a MIMO environment, channel estimation needs to be more accurate than in a SISO environment. To improve CTF estimation, this paper applies the DDP to 2x2 MIMO with spatial multiplexing environment to study CTF generation method that is more accurate than conventional CTF estimation methods.

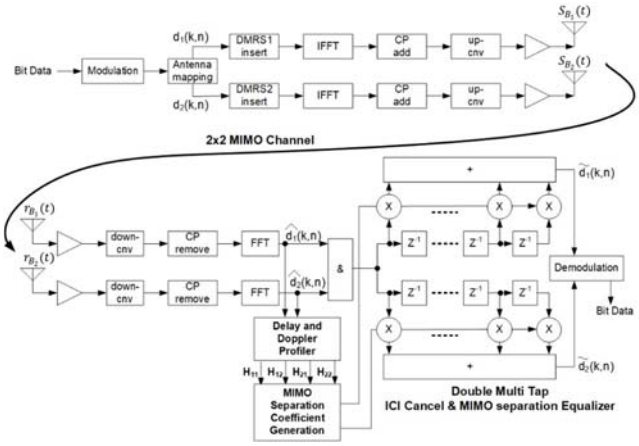

Fig. 4: Physical layer of 5G communication system for 2x2 MIMO

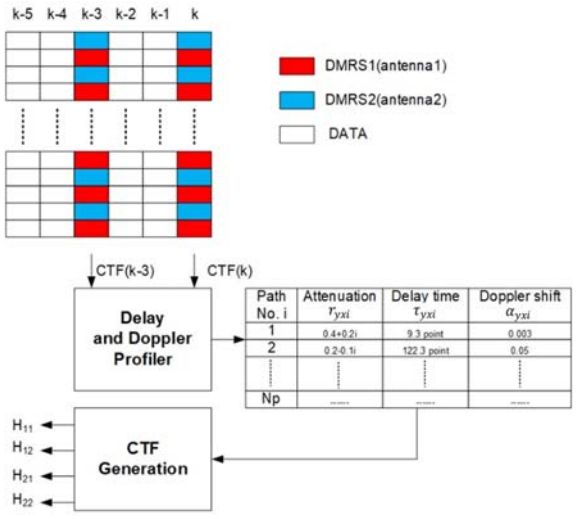

Fig. 5: Delay and Doppler Profiler based CTF estimator for 2x2 MIMO

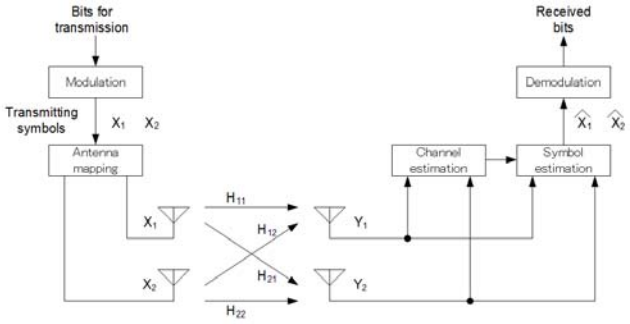

Fig. 6: Basic representation of 2x2 MIMO system

B) ICI Cancellation based on Delay and Doppler Profiler for 2x2 MIMO

References [4-6] describe detail methods of Delay and Doppler Profile (DDP) based CTF estimation using pilot signals embedded in OFDM sub-carriers. Fig. 5 shows a block diagram of proposed DDP CTF generation. The upper side of the figure represents the Time-Frequency structure of sub-carriers with time-domain symbol index k. The DDP estimates each N_P, multipath component waves to receiving each antenna. Each analyzed component can be characterized using three parameters such as Attenuation r_{yxi}, Propagation Delay time τ_{yxi}, and normalized Doppler shift α_{yxi} with transmit antenna number x, receive antenna number y, and wave component index i. Here the Attenuation r_{yxi} is complex value including amplitude attenuation and phase rotation and the normalized Doppler shift is normalized by sub-carrier spacing f_0 such as $\alpha_{yxi} = fd_i/f_0$. Using the symbol k measured $CTF_{yx}(k)$ and symbol $k-3$ measured $CTF_{yx}(k-3)$, the DDP detects N_P sets of those three parameters.

5G baseband transmitting for 2x2 MIMO signals $s_{B_1}(t)$ and $s_{B_2}(t)$ can be expressed as Equations (1a) and (1b). As shown in Fig. 4, $s_{B_1}(t)$ represents the signal from transmitting antenna number 1, and $s_{B_2}(t)$ represents the signal from transmitting antenna number 2.

$$s_{B1}(t) = \sum_{m=-\infty}^{\infty} g(t-mT_s) \cdot \sum_{n=0}^{N-1} d_1(m,n) e^{j2\pi n f_0 (t-mT_s)} \quad \cdots (1a)$$

$$s_{B2}(t) = \sum_{m=-\infty}^{\infty} g(t-mT_s) \cdot \sum_{n=0}^{N-1} d_2(m,n) e^{j2\pi n f_0 (t-mT_s)} \quad \cdots (1b)$$

$$T_s = \frac{1}{f_0} + T_g \quad \cdots (2)$$

$$g(t) = \begin{cases} 1 & -T_g \leqq t < 1/f_0 \\ 0 & otherwise \end{cases} \quad \cdots (3)$$

where, N is the number of sub-carriers, f_0 is the sub-carrier spacing, T_s is symbol length as defined in equation (2), $d_1(m,n)$ and $d_2(m,n)$ are data symbols of sub-carrier index n at the m^{th} OFDM symbol. By assuming the transmission channel has N_P delay paths, the received baseband signals can be written as Equations (4a) and (4b).

$$r_{B1}(t) = \sum_{p=1}^{N_P} r_{11p}\, s_{B1}(t-\tau_{11p}) e^{j2\pi\Delta f_{11p}(t-\tau_{11p})} + \sum_{p=1}^{N_P} r_{12p}\, s_{B2}(t-\tau_{12p}) e^{j2\pi\Delta f_{12p}(t-\tau_{12p})} \quad \cdots (4a)$$

$$r_{B2}(t) = \sum_{p=1}^{N_P} r_{21p}\, s_{B1}(t-\tau_{21p}) e^{j2\pi\Delta f_{21p}(t-\tau_{21p})} + \sum_{p=1}^{N_P} r_{22p}\, s_{B2}(t-\tau_{22p}) e^{j2\pi\Delta f_{22p}(t-\tau_{22p})} \quad \cdots (4b)$$

$$t = \frac{i}{Nf_0} + kT_s \quad \cdots (5)$$

where, r_{yxp}, τ_{yxp} and Δf_{yxp} are attenuation, relative delay and Doppler-shift of p^{th} path when the signal from transmit antenna number x is received at receive antenna number y, respectively. After sampling of $r_{B_1}(t)$ and $r_{B_1}(t)$ by using Equation (5) with sampling index i and OFDM symbol number k, the block of samples is de-modulated by DFT to generate data symbol $\widehat{d_1}(k,l)$ and l $\widehat{d_2}(k,l)$ as expressed in Equations (6a) and (6b).

$$\widehat{d_1}(k,l) = h_{11}(k,l,l)d_1(k,l) + \sum_{\substack{n=0 \\ n\neq l}}^{N-1} h_{11}(k,l,n)d_1(k,n) + h_{12}(k,l,l)d_2(k,l) + \sum_{\substack{n=0 \\ n\neq l}}^{N-1} h_{12}(k,l,n)d_2(k,n) + w_1(k,l) \quad \cdots (6a)$$

$$\widehat{d_2}(k,l) = h_{21}(k,l,l)d_1(k,l) + \sum_{\substack{n=0 \\ n\neq l}}^{N-1} h_{21}(k,l,n)d_1(k,n) + h_{22}(k,l,l)d_2(k,l) + \sum_{\substack{n=0 \\ n\neq l}}^{N-1} h_{22}(k,l,n)d_2(k,n) + w_2(k,l) \quad \cdots (6b)$$

where $w_1(k,l)$ and $w_2(k,l)$ are additive noise that corresponds to the l^{th} sub-carrier in the k^{th} OFDM symbol and $h_{yx}(k,l,n)$ is the channel transfer function from symbol $d_1(k,n)$ and $d_2(k,n)$ to the l^{th} sub-carrier. If $n \neq l$, $h_{yx}(k,l,n)$ represents the influence of ICI (Inter Carrier Interference). $h_{yx}(k,l,n)$ can be expressed as Equations (7), (8a) and (8b).

$$h_{yx}(k,l,n) = \sum_{p=1}^{N_P} h_{yxp}(k,l,n) \quad \cdots (7)$$

$$h_{yxp}(k,l,n) = \frac{sinc(A)}{sinc(\frac{A}{N})} \cdot e^{j\frac{\pi(N-1)A}{N}} \cdot r_{yxp} \cdot e^{-j\frac{2\pi(n+\alpha_{yxp})\tau'_{yxp}}{N}} \cdot e^{j\frac{2\pi k(N+GI)\alpha_{yxp}}{N}} \quad \cdots (8a)$$

$$A = n - l + \alpha_{yxp} \quad \cdots (8b)$$

where $\alpha_{yxp} = \Delta f_{yxp}/f_0$ is normalized frequency offset of p^{th} path when the signal from transmit antenna number x is received at receive antenna number y, respectively.

The parameters of channel transfer function $h_{yx}(k,l,n)$ are estimated so as to minimize the mean square error shown in Equation (9).

$$E_{yx}(k) = \sum_{l=P} \left\{ \left| CTF_{yx}(k,l) - h_{yx}(k,l,l) \right|^2 + \left| CTF_{yx}(k-3,l) - h_{yx}(k-3,l,l) \right|^2 \right\} \quad \cdots (9)$$

where $\Sigma_{l=P}$ means that the summation is performed as long as l is DMRS pilot symbol.

In order to simplify the problem, it is supposed that the channel model contains one path at the first. In this case, criterion is rewritten as Equation (10).

$$\begin{aligned} &E_{yx1}(k) \\ &= \sum_{l=P} \left\{ \left| CTF_{yx}(k,l) - f(\alpha_{yx1}) r_{yx1} \cdot e^{-j\frac{2\pi(l+\alpha_{yx1})\tau'_{yx1}}{N}} \right|^2 \right. \\ &+ \left| CTF_{yx}(k-3,l) \right. \\ &\left. \left. - f(\alpha_{yx1}) r_{yx1} \cdot e^{-j\frac{2\pi(l+\alpha_{yx1})\tau'_{yx1}}{N}} \cdot e^{j\frac{-2\pi 3(N+GI)\alpha_{yx1}}{N}} \right|^2 \right\} \quad \cdots (10) \end{aligned}$$

here, $f(\alpha_{yx1})$ is written as Equation (11).

$$f(\alpha_{yx1}) = \frac{sinc(\alpha_{yx1})}{sinc\left(\frac{\alpha_{yx1}}{N}\right)} \cdot e^{j\frac{\pi(N-1)\alpha_{yx1}}{N}} \cdot e^{j\frac{2\pi k(N+GI)\alpha_{yx1}}{N}} \quad \cdots (11)$$

One of the necessary conditions to minimize $E_{yx1}(k)$ with regard to r_{yx1}, τ'_{yx1} (relative delay time in sampling points) and α_{yx1} is that its partial derivative of r_{yx1} has zero value. With this condition, r_{yx1} can be shown as Equations (12a) and (12b).

$$r_{yx1} = \frac{S^*_{yx\_k} + e^{j\frac{2\pi 3(N+GI)\alpha_{yx1}}{N}} S^*_{yx\_k-3}}{2 \cdot f(\alpha_{yx1}) e^{-j\frac{2\pi\alpha_{yx1}\tau'_{yx1}}{N}}} \quad \cdots (12a)$$

here,

$$S_{yx\_k} = \sum_{l=P} CTF^*_{yx}(k,l)\, e^{-j\frac{2\pi l\tau'_{yx1}}{N}} \quad \cdots (12b)$$

By calculate more as shown in reference [4-6], α_{yx1} is calculated from τ'_{yx1} as Equation (13).

$$\alpha_{yx1} = \frac{1}{\frac{2\pi 3(N+GI)}{N}} arctan\left[\frac{\Im(S^*_{yx\_k} \cdot S_{yx\_k-3})}{\Re(S^*_{yx\_k} \cdot S_{yx\_k-3})} \right] \quad \cdots (13)$$

Consequently, once τ'_{yx1} is determined, r_{yx1} and α_{yx1} are easily obtained from Equations (12a) and (13), respectively. In this proposed method, τ'_{yx1} is changed by $1/(2Nf_0)$ (twice of sampling frequency) and rough estimation is first obtained. And this rough estimation is modified to more precise value using Newton method as described in references [4-6].

According to the computation above, $h_{yx1}(k,l,n)$ can be obtained using Equations (8a) and (8b). Then, measured $CTF_{yx}(k,l)$ and $CTF_{yx}(k-3,l)$ are updated to $CTF_{yx}(2,k,l)$ and $CTF_{yx}(2,k-3,l)$ by subtracting $h_{yx1}(k,l,n)$ and $h_{yx1}(k-3,l,n)$ respectively. By removing the influence of the first estimated path from the cost function $E_{yx1}(k)$, the following criterion $E_{yx2}(k)$ can be obtained such as Equation (14).

$$\begin{aligned} &E_{yx2}(k) \\ &= \sum_{l=P} \left\{ \left| CTF_{yx}(2,k,l) - f(\alpha_{yx2}) r_{yx2} \cdot e^{-j\frac{2\pi(l+\alpha_{yx2})\tau'_{yx2}}{N}} \right|^2 \right. \\ &+ \left| CTF_{yx}(2,k-3,l) \right. \\ &\left. \left. - f(\alpha_{yx2}) r_{yx2} \cdot e^{-j\frac{2\pi(l+\alpha_{yx2})\tau'_{yx2}}{N}} \cdot e^{j\frac{-2\pi 3(N+GI)\alpha_{yx2}}{N}} \right|^2 \right\} \quad \cdots (14) \end{aligned}$$

Since $E_{yx2}(k)$ contains the influence of other paths, the second path can be estimated using the same procedure in the previous section. By repeating this operation by the number of paths in the channel model, N_p sets of those three parameters can be obtained as shown in Fig. 5, and Fig. 6.

After all, complete channel transfer function $h_{yx}(k,l,n)$ can be generated. Since most energy of ICI is concentrated in the neighborhood of sub-carrier index, the ICI terms which do not significantly affect $\hat{d}_1(k,l)$ and $\hat{d}_2(k,l)$ in (6a) and (6b) can be neglected and it is assumed as (15).

$$h_{yx}(k,l,n) = 0 \quad when \quad |l-n| > \frac{NumCOL-1}{2} \quad \cdots (15)$$

where, $NumCOL$ is the number of neighborhood sub-carrier taken into account against l^{th} sub-carrier. By considering the reverse operation of the ICI effect by $h(k,l,n)$, Multi Tap ICI Canceling Equalizer has been implemented as shown in Fig. 4. as a Fixed Impulse Response Filter.

The CTF needs to be calculated for the number of combinations of the number of transmit and receive antennas. Therefore, in the case of 2x2 MIMO, the number of CTF calculations is required for four paths H_{11}, H_{12}, H_{21} and H_{22} as shown in Fig. 6. This can be expressed in the theoretical equation as shown in Equation (16) below.

$$\begin{bmatrix} Y_1 \\ Y_2 \end{bmatrix} = \begin{bmatrix} H_{11} & H_{12} \\ H_{21} & H_{22} \end{bmatrix} \begin{bmatrix} X_1 \\ X_2 \end{bmatrix} + \begin{bmatrix} n_1 \\ n_2 \end{bmatrix} \quad \cdots (16)$$

The equation for channel equalization using the channel estimation results of the received signal is shown in Equation (17).

$$\begin{bmatrix} \widehat{X_1} \\ \widehat{X_2} \end{bmatrix} \cong \begin{bmatrix} H_{11} & H_{12} \\ H_{21} & H_{22} \end{bmatrix}^{-1} \begin{bmatrix} Y_1 \\ Y_2 \end{bmatrix} \quad \cdots (17)$$

Assuming the number of TAPs ($NumCOL$) for the multi-tap ICI cancel equalizer is 3taps, Equations (6a) and (6b) can be rewritten as follows.

$$\begin{bmatrix}\widehat{d_1}(k,l-1)\\ \widehat{d_1}(k,l)\\ \widehat{d_1}(k,l+1)\end{bmatrix} = \begin{bmatrix}h_{11}(k,l-1,l-1) & h_{11}(k,l-1,l) & h_{11}(k,l-1,l+1)\\ h_{11}(k,l,l-1) & h_{11}(k,l,l) & h_{11}(k,l,l+1)\\ h_{11}(k,l+1,l-1) & h_{11}(k,l+1,l) & h_{11}(k,l+1,l+1)\end{bmatrix}\begin{bmatrix}d_1(k,l-1)\\ d_1(k,l)\\ d_1(k,l+1)\end{bmatrix} + \begin{bmatrix}h_{12}(k,l-1,l-1) & h_{12}(k,l-1,l) & h_{12}(k,l-1,l+1)\\ h_{12}(k,l,l-1) & h_{12}(k,l,l) & h_{12}(k,l,l+1)\\ h_{12}(k,l+1,l-1) & h_{12}(k,l+1,l) & h_{12}(k,l+1,l+1)\end{bmatrix}\begin{bmatrix}d_2(k,l-1)\\ d_2(k,l)\\ d_2(k,l+1)\end{bmatrix} + \begin{bmatrix}w_1(k,l-1)\\ w_1(k,l)\\ w_1(k,l+1)\end{bmatrix} \cdots (18a)$$

$$\begin{bmatrix}\widehat{d_2}(k,l-1)\\ \widehat{d_2}(k,l)\\ \widehat{d_2}(k,l+1)\end{bmatrix} = \begin{bmatrix}h_{21}(k,l-1,l-1) & h_{21}(k,l-1,l) & h_{21}(k,l-1,l+1)\\ h_{21}(k,l,l-1) & h_{21}(k,l,l) & h_{21}(k,l,l+1)\\ h_{21}(k,l+1,l-1) & h_{21}(k,l+1,l) & h_{21}(k,l+1,l+1)\end{bmatrix}\begin{bmatrix}d_1(k,l-1)\\ d_1(k,l)\\ d_1(k,l+1)\end{bmatrix} + \begin{bmatrix}h_{22}(k,l-1,l-1) & h_{22}(k,l-1,l) & h_{22}(k,l-1,l+1)\\ h_{22}(k,l,l-1) & h_{22}(k,l,l) & h_{22}(k,l,l+1)\\ h_{22}(k,l+1,l-1) & h_{22}(k,l+1,l) & h_{22}(k,l+1,l+1)\end{bmatrix}\begin{bmatrix}d_2(k,l-1)\\ d_2(k,l)\\ d_2(k,l+1)\end{bmatrix} + \begin{bmatrix}w_2(k,l-1)\\ w_2(k,l)\\ w_2(k,l+1)\end{bmatrix} \cdots (18b)$$

Equations (18a) and (18b) can also be rewritten using the matrix as follows.

$$\begin{bmatrix}\begin{pmatrix}\widehat{d_1}(k,l-1)\\ \widehat{d_1}(k,l)\\ \widehat{d_1}(k,l+1)\end{pmatrix}\\ \begin{pmatrix}\widehat{d_2}(k,l-1)\\ \widehat{d_2}(k,l)\\ \widehat{d_2}(k,l+1)\end{pmatrix}\end{bmatrix} = \begin{bmatrix}\boldsymbol{H_{11}} & \boldsymbol{H_{12}}\\ \boldsymbol{H_{21}} & \boldsymbol{H_{22}}\end{bmatrix} \times \begin{bmatrix}\begin{pmatrix}d_1(k,l-1)\\ d_1(k,l)\\ d_1(k,l+1)\end{pmatrix}\\ \begin{pmatrix}d_2(k,l-1)\\ d_2(k,l)\\ d_2(k,l+1)\end{pmatrix}\end{bmatrix} \cdots (19a)$$

here,

$$\boldsymbol{H_{yx}} = \begin{pmatrix}h_{yx}(k,l-1,l-1) & h_{yx}(k,l-1,l) & h_{yx}(k,l-1,l+1)\\ h_{yx}(k,l,l-1) & h_{yx}(k,l,l) & h_{yx}(k,l,l+1)\\ h_{yx}(k,l+1,l-1) & h_{yx}(k,l+1,l) & h_{yx}(k,l+1,l+1)\end{pmatrix} \cdots (19b)$$

The equalizer of the 2x2 MIMO receiver can be equated as follows. Using the DDP algorithm, Attenuation r_{yxi}, Propagation Delay time τ_{yxi}, and normalized Doppler shift α_{yxi} for wave component index i of the arrival path of each receiving antenna are determined and used as CTFs H_{11}, H_{12}, H_{21} and H_{22}. Since this paper assumes use in 2x2MIMO, the inverse matrix is calculated by applying the formulas, resulting in the following Equation (20).

$$\begin{bmatrix}\begin{pmatrix}\widehat{d_1}(k,l-1)\\ \widehat{d_1}(k,l)\\ \widehat{d_1}(k,l+1)\end{pmatrix}\\ \begin{pmatrix}\widehat{d_2}(k,l-1)\\ \widehat{d_2}(k,l)\\ \widehat{d_2}(k,l+1)\end{pmatrix}\end{bmatrix} = \begin{bmatrix}\boldsymbol{H_{11}} & \boldsymbol{H_{12}}\\ \boldsymbol{H_{21}} & \boldsymbol{H_{22}}\end{bmatrix}^{-1} \times \begin{bmatrix}\begin{pmatrix}\widehat{d_1}(k,l-1)\\ \widehat{d_1}(k,l)\\ \widehat{d_1}(k,l+1)\end{pmatrix}\\ \begin{pmatrix}\widehat{d_2}(k,l-1)\\ \widehat{d_2}(k,l)\\ \widehat{d_2}(k,l+1)\end{pmatrix}\end{bmatrix} \cdots (20)$$

III. Computer Simulations

Since the actual test environment is not yet available, computer simulations were used to simulate the environment. Fig. 7 shows a computer simulated running linear motor train situation. Nearby Base Station (gNB: g Node B in 5G notation) antennas are located from the train rail by D (m). In a Single Frequency Network (SFN), the same DL signal is transmitted from antennas in different each gNB. The distance between the center of the two Tx antennas of the gNB and the center of the two Rx antennas at the receiver is 300 m. The center position of the two Rx antennas is Xr(t) on the horizontal X axis as shown in Fig. 7. Also, the distance between the Tx antennas is defined as td, and the distance between the Rx antennas is defined as rd. The distances between two Tx antennas and the Rx antenna are $L1_{yx}(t)$, and $L2_{yx}(t)$ $(y = 1,2,\ x = 1,2)$ as shown in the figure (Fig. 7).

More detail of simulation parameters is listed in Table 2. Assumed Radio passband frequency is 3.9 GHz. In the simulation, moving train will start receiving 1 frames of DL signal with Xr(t=0) = -50 m. Path1-4 DL signal comes from forward antenna with varying length $L1_{11}(t)$, $L1_{12}(t)$, $L1_{21}(t)$, $L1_{22}(t)$ with relative amplitude gain = 1.0. Path5-8 DL signal comes from backside with $L2_{11}(t)$, $L2_{12}(t)$, $L2_{21}(t)$, $L2_{22}(t)$ distance with relative amplitude gain = 0.5. Bit Error Rate (BER) is measured in lower frequency 90 CRBs as shown in Fig. 3. The BER was obtained by adding Additive White Gaussian Noise (AWGN) to the signal received as a composite wave of the 2gNB-derived DL signal, varying from -10 dB to 50 dB in 2 dB steps.

The conventional method shall obtain the channel estimates in the frequency and time directions for each slot by performing the following two steps. As the first step, a half-band FIR (Finite Impulse Response) filter is passed

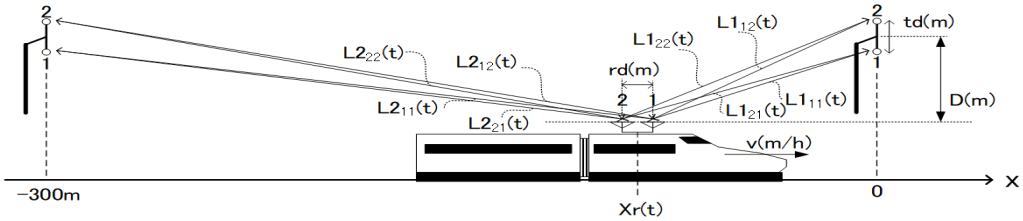

Fig. 7: Simulation model of train moving situation for 2x2 MIMO environment

through the carrier for which channel estimation was performed for the DMRS symbols, and channel estimation is performed in the frequency domain to obtain channel estimates for each carrier for one symbol. This process is performed for four symbols containing DMRS for each slot. In the second step, linear interpolation is performed between the two symbols for which the channel estimate of the frequency location was obtained. By repeating the second step for each DMRS symbol, time direction channel estimation can be performed for symbols that do not contain DMRS. The advantage of the conventional method is that it is computationally less expensive than the proposed DDP algorithm, but its disadvantages are that it requires several consecutive RB assignments to improve channel estimation accuracy and that it is difficult to perform filter completion at both ends of the RBs used, so separate processing is necessary.

The proposed DDP-based ICI cancellation equalizer is based on the estimation of the attenuation r_{yxi}, propagation delay time τ_{yxi}, and normalized Doppler shift α_{yxi} in the arriving wave for each CTF, one pass at a time, as described in Section II, subsection B, followed by a Fixed Impulse Response Filter, followed by equalization with a multi-tap ICI canceller using a Fixed Impulse Response filter.

The number of taps in the fixed impulse response filter of the ICI canceller equalizer, $NumCOL$=1, corresponds to the condition where the number of adjacent subcarriers is not considered, but the computational complexity is about 16 times that of the conventional method. 8 patterns from $NumCOL = 1$ to $NumCOL = 63$ were used in the computer simulations; CNR versus BER data acquisition was performed for these eight patterns while varying the $NumCOL$ factor. We performed computer simulations of the conventional method and the proposed method for these eight patterns while varying the $NumCOL$ factor for the proposed method, and obtained CNR vs. BER data.

Simulated results for QPSK / 16QAM / 64QAM / 256QAM BER vs Carrier to Noise Ratio (CNR) with moving speed 500km/h were shown in Figs. 8-11. In each figure, (a) shows the simulation results of the conventional scheme using the basic DMRS pattern and the proposed scheme using the basic DMRS pattern and varying $NumCOL$ values in a 3GPP standard-compliant downlink signal in 5G. On the other hand, in the specifications after 3GPP Release 16, the transmit DMRS pattern can be changed for each antenna. To confirm the effect of improving the characteristics by adding a device to further improve the cross-correlation characteristics by changing the DMRS pattern for each transmitting antenna, (b) shows the simulation results when the DMRS pattern is changed for each transmitting antenna.

Simulation results show that the proposed DDP-based ICI canceller scheme outperforms conventional schemes, even at a moving speed of 500 km/h, regardless of the modulation scheme and whether the DMRS pattern between the two transmit antennas is common or independent, by increasing the $NumCOL$ value to about 31, This indicates that BER can be significantly improved by increasing the $NumCOL$ value to about 31. Here, $NumCOL = 1$ corresponds to a DDP-based channel equalizer without an ICI canceller, which corresponds to the algorithm presented in reference [7]. In the conventional method, there was little BER improvement regardless of the DMRS pattern.

Table 2: Simulation Parameters

Parameters	**Value**
RF passband frequency	3.9 GHz
Modulation	QPSK / 16QAM / 64QAM / 256QAM
RX moving speed	0 km/h ~ 500km/h, (100km/h step)
CNR	Add to AWGN -10 dB ~ 50 dB, (2 dB step)
Number of Frames	1 Frames (10 ms, 20 slots)
Used number of CRBs	90 CRBs (1080 Sub-carriers)
Channel	2x2 MIMO with Spatial Multiplexing, 8-path Single Frequency Network
Path Group 1 ($L1_{11}(t)$, $L1_{12}(t)$, $L1_{21}(t), L1_{22}(t)$)	Distance = ~50 meters Amp gain = 1.0
Path Group 2 ($L2_{11}(t)$, $L2_{12}(t)$, $L2_{21}(t), L2_{22}(t)$)	Distance = ~250 meters Amp gain = 0.5
Tx Antenna Installation Height (D)	D = 2.0 meters
Tx Antenna Distance (td)	td = 0.5 meters
Rx Antenna Distance (rd)	rd = 0.05 meters
Number of Fixed Impulse Response Filter Taps of ICI Canceling Equalizer ($NumCOL$)	8patterns (1, 3, 5, 7, 15, 31, 45, 63)

Fig. 8(a) and Fig. 8(b) show a comparison of QPSK modulation. Fig. 8(a), which uses the same DMRS pattern across transmit antennas, requires $NumCOL = 3$ or more to be error-free, while Fig. 8(b), which changes the DMRS pattern for each transmit antenna, shows that $NumCOL = 1$ is sufficient to be error-free. In Fig. 9(a) and Fig. 9(b), which are graphs for 16QAM modulation, if we focus on the graph for $NumCOL = 31$, we can see that changing the DMRS pattern for each transmit antenna improves the BER by two orders of magnitude. As the modulation value increases, the improvement in BER becomes smaller, but we can see that BER improves from QPSK to 256QAM. The paper concludes that $NumCOL = 31$ is the optimal value for the DDP algorithm, which is consistent with the conclusions for DDP-based multi-tap channel equalization in a SISO environment presented in reference [1].

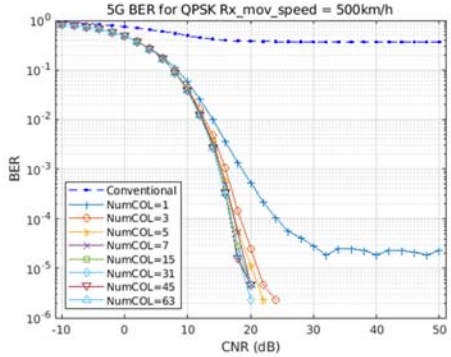

(a) DMRS pattern is the same between transmit antennas

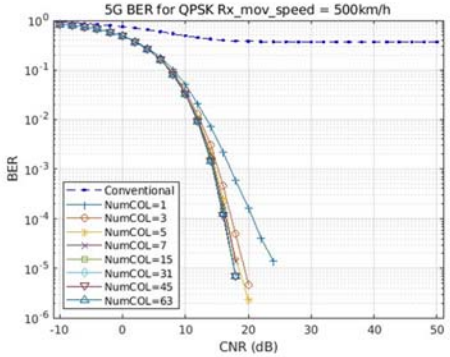

(b) DMRS pattern changed for each transmit antenna

Fig. 8: BER vs CNR (dB) for 2x2 MIMO QPSK modulation

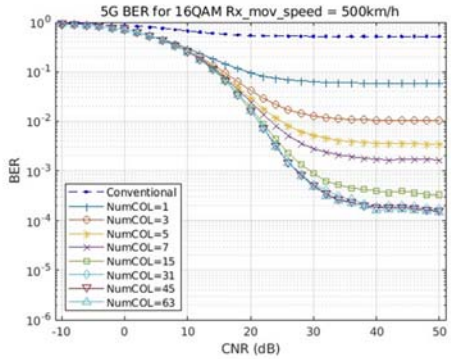

(a) DMRS pattern is the same between transmit antennas

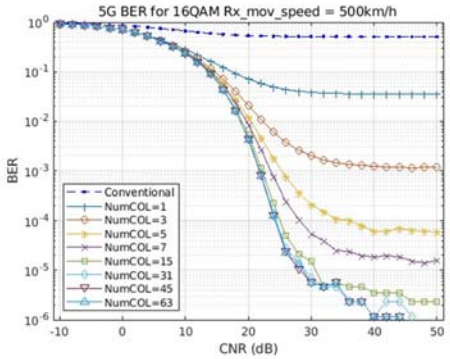

(b) DMRS pattern changed for each transmit antenna

Fig. 9: BER vs CNR (dB) for 2x2 MIMO 16QAM modulation

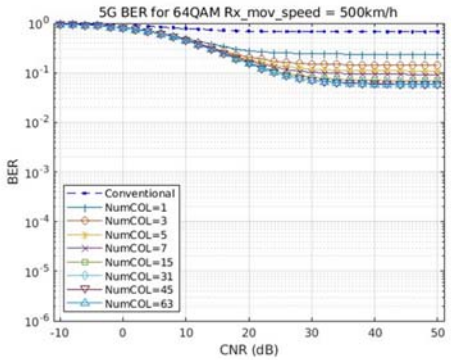

(a) DMRS pattern is the same between transmit antennas

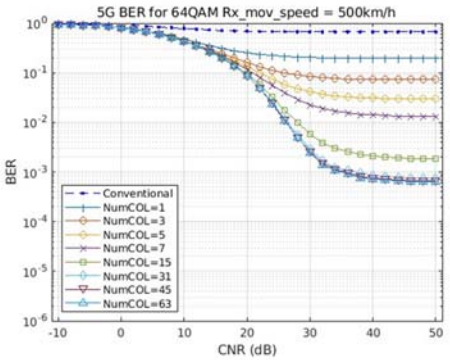

(b) DMRS pattern changed for each transmit antenna

Fig. 10: BER vs CNR (dB) for 2x2 MIMO 64QAM modulation

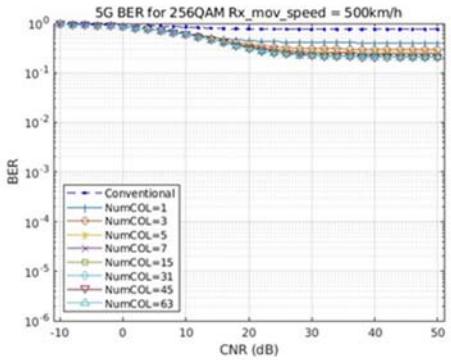

(a) DMRS pattern is the same between transmit antennas

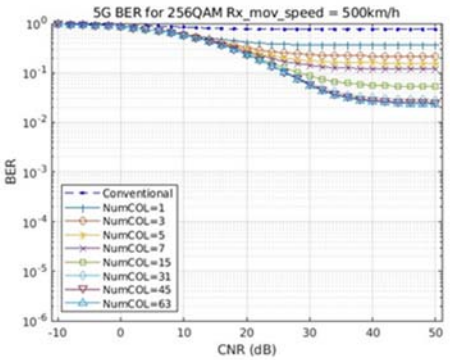

(b) DMRS pattern changed for each transmit antenna

Fig. 11: BER vs CNR (dB) for 2x2 MIMO 256QAM modulation

Finally, Figs. 12 and 13 show the simulation results when the parameters are changed from a travel speed of 0 km/h to 500 km/h under the condition of changing the DMRS pattern for each transmit antenna. In this case, the $NumCOL$ value of 31 was used, which was the performance limit based on the results of Figs. 8-11. It shows that the BER is better when the DMRS pattern is changed for every two transmit antennas at all speeds from 0 km/h to 500 km/h of movement. Fig. 12(b) shows that the 16QAM modulation scheme is fully usable in a spatial multiplexing 2x2 MIMO environment. Fig. 13(b) also shows that the 2x2 MIMO 64QAM modulation scheme in combination with LDPC and other channel decoding can be used in a 500 km/h environment. At a moving speed of 500 km/h, BER is improved by two orders of magnitude.

IV. Conclusion

Delay and Doppler Profiler (DDP) based spatial multiplexing 2x2 MIMO Channel Estimator is proposed targeting 500km/h train support and it is successfully implemented in signal processing simulation system. Simulated performances are compared with the conventional frequency domain using half band interpolation filter and time domain linear interpolated estimator.

Simulation results show that QPSK modulation in a space-multiplexed 2x2 MIMO environment can be used under severe channel conditions such as 500 km/h under 8-path inverse Doppler shift conditions with a channel estimator using the DDP algorithm based on the proposed method.

In addition, by applying the DMRS pattern change per transmit antenna added after Release 16 of the 5G standard, the error rate after channel decoding under 500 km/h moving speed can be kept low even for 16QAM modulation and 64QAM modulation in a spatial multiplexing 2x2 MIMO environment. However, the improvement rate for 256QAM modulation is small.

Adaptive modulation such that 16QAM modulation is the upper limit of the modulation scheme during high-speed movement and 64QAM modulation is the upper limit during low-speed movement would reduce the retransmission probability and improve total throughput.

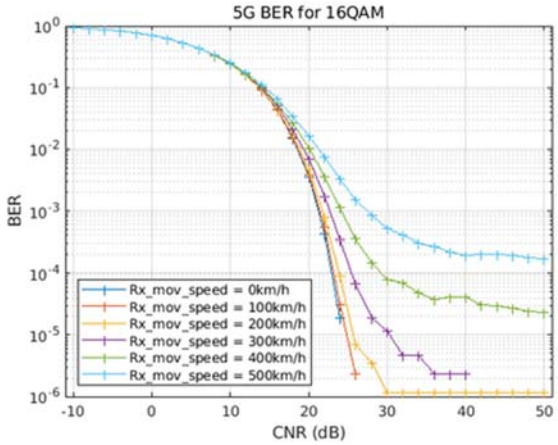

(a) DMRS pattern is the same between transmit antennas

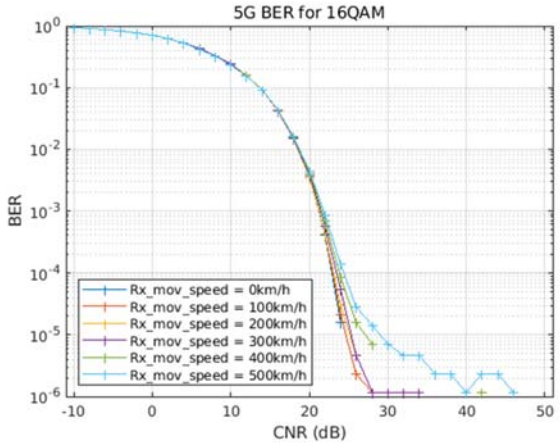

(b) DMRS pattern changed for each transmit antenna

Fig. 12: BER vs Moving Speed for 2x2 MIMO 16QAM (NumCOL=31)

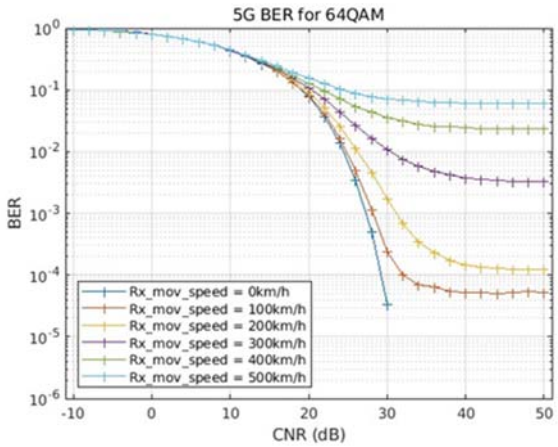

(a) DMRS pattern is the same between transmit antennas

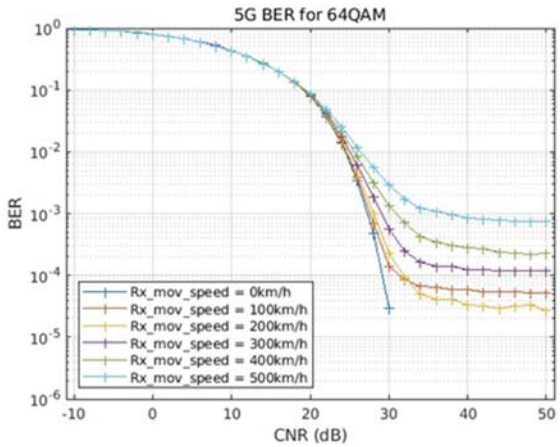

(b) DMRS pattern changed for each transmit antenna

Fig. 13: BER vs Moving Speed for 2x2 MIMO 64QAM (NumCOL=31)

References

[1] Suguru Kuniyoshi, Rie Saotome, Shiho Oshiro and Tomohisa Wada, "An ICI Canceling 5G system receiver for 500km/h linear motor car," IJCSNS International Journal of Computer Science and Network Security, VOL.23, No.6, pp.27-34, June 2023.

[2] 3GPP TS38.211 V17.4.0: "3rd Generation Partnership Project; Technical Specification Group Radio Access Network; NR; Physical channels and modulation" Dec. 2022.

[3] Erik Dahlman, Stefan Parkvall, Johan Sköld (2021). *5G NR THE NEXT GENERATION WIRELESS ACCESS TECHNOLOGY SECOND EDITION.* Academic Press.

[4] Mitsuru Nakamura, Makoto Itami, Kohji Itoh and Hamid Aghvami, "ICI Cancellation Technique based on Estimating Delay and Doppler Profile in OFDM Reception," The Institute of Image Information and Television Engineers, Vol. 56, No. 12, pp.1951-1958 (2002).

[5] Mitsuru Nakamura, Masahiro Fujii, Makoto Itami and Kohji Itoh, "MMSE ICI Canceller for OFDM Mobile Reception," The Institute of Image Information and Television Engineers, Vol. 58, No. 1, pp.83-90 (2004).

[6] Akito Yamazaki, Mitsuru Nakamura, Masahiro Fujii, Makoto Itami, Kohji Itoh and Hiroki Ohta, "A Study on Improving Performance of an OFDM ICI Canceller," The Institute of Image Information and Television Engineers, Vol. 58, No. 1, pp.94-101 (2005).

[7] Suguru Kuniyoshi, Rie Saotome, Shiho Oshiro and Tomohisa Wada, "Delay and Doppler Profiler based Channel Transfer Function estimation for 2x2 MIMO Receivers in 5G system targeting a 500km/h linear motor car," IJCSNS International Journal of Computer Science and Network Security, VOL.23, No.9, pp.8-16, September 2023.

Suguru Kuniyoshi received the B.E. and M.E. degrees, from the University of the Ryukyus, Okinawa, Japan in 2004 and 2006, respectively. He joined Magna Design Net, Inc. in 2006 and has engaged with digital signal processing design of modulator and demodulator part for a Wireless LAN, WiMAX, 4G-LTE, 5G-NR, and Underwater Acoustic communication. Currently he is the Engineering Manager of the Development Department at Magna Design Net, Inc.

Rie Saotome received the B.E. and M.E. degree from Tokyo University of technology, Tokyo, Japan in 1999 and 2001, respectively. She received Dr. Eng. degree from University of the Ryukyus in 2016. From 2004 to 2016, she was a part-time lecturer at Univ. of the Ryukyus, Okinawa Univ., Meio Univ. and Okinawa Polytechnic College. She joined Magna Design Net, Inc. in 2016. Her research interest includes Wireless communications systems, 5G-NR, Underwater Acoustic communication, and Rain attenuation.

Shiho Oshiro received the B.E. and M.E. degrees, from the University of the Ryukyus, Okinawa, Japan in 2018 and 2020, respectively. She received the Dr. Eng. degree from University of the Ryukyus in 2023. She has been an assistant professor at University of the Ryukyus since 2023. She has experienced short-term study abroad at Madan Mohan Malaviya University of Technology (MMMUT) Gorakhpur and Atal Bihari Vajpayee-Indian Institute of Information Technology and Management (ABV-IIITM) Gwalior in India, Institute of Technology of Cambodia (ITC) in Cambodia, and National Taiwan University of Science and Technology (Taiwan Tech). Her research interest includes Underwater OFDM Acoustic communication systems, developed Underwater Acoustic OFDM wireless communication systems, Underwater Acoustic Positioning systems targeting for Underwater Drone controls, Flight Control for Underwater Drone automatically controls, and Autoencoder for OFDM communication system.

Tomohisa Wada received B.S. degree in electronic engineering from Osaka University, Osaka, Japan, in 1983, M.S.E.E. degree from Stanford University, Stanford CA, in 1992, and Ph.D. in electronic engineering from Osaka University in 1994. He joined the ULSI Laboratory, Mitsubishi Electric Corp. Japan in 1983 and engaged in the research and development of VLSI such as High-speed Static Random-access memories, Cache memories for Intel MPUs in 16 years. Since 2001, he has been a Professor at the Department of Information Engineering, the University of the Ryukyus, Okinawa, Japan. In 2001, He was the founding member of Magna Design Net, Inc., which is a fab-less LSI design Company for communication related digital signal processing such as OFDM. Currently, he is also the chief scientist of Magna Design Net, Inc. who is engaging in the research and development of a terrestrial video broadcasting receiver, a wireless LAN, WiMAX, 4G-LTE and 5G systems. After 2009, he also started Underwater OFDM Acoustic communication systems and developed Underwater Acoustic OFDM wireless communication systems and Underwater Acoustic Positioning systems targeting for Underwater Drone controls.